journal of the mechanical behavior of biomedical materials 163 (2025) 106865

Contents lists available at ScienceDirect

Journal of the Mechanical Behavior of Biomedical Materials

journal homepage: www.elsevier.com/locate/jmbbm

Poroelastic and viscoelastic properties of soft materials determined from AFM force relaxation and force-distance curves

Stéphane Cuenot [a,*], Arnaud Fillaudeau [a], Tina Briolay [b], Judith Fresquet [b], Christophe Blanquart [b], Eléna Ishow [c], Agata Zykwinska [d]

[a] Nantes Université, CNRS, Institut des Matériaux de Nantes Jean Rouxel, IMN, F-44000, Nantes, France
[b] Nantes Université, Inserm UMR 1307, CNRS UMR 6075, Université d'Angers, CRCI2NA, F-44000, Nantes, France
[c] Nantes Université, CNRS, CEISAM, UMR 6230, F-44000, Nantes, France
[d] Ifremer MASAE Microbiologie Aliment Santé Environnement, F-44000, Nantes, France

ARTICLE INFO

Keywords:
Viscoelasticity
Poroelasticity
Hydrogels
Cells
Power-law rheology model
Spherical AFM tips

ABSTRACT

In the field of tissue engineering, determining the mechanical properties of hydrogels is a key prerequisite to develop biomaterials mimicking the properties of the extracellular matrix. In mechanobiology, understanding the relationships between the mechanical properties and physiological state of cells is also essential. Time-dependent mechanical characterization of these soft materials is commonly achieved by atomic force microscopy (AFM) experiments in liquid environment. However, the determination of an appropriate model to correctly interpret the experimental data is often missing, making it difficult to extract quantitative mechanical properties. Here, force relaxation and force-distance curves were combined to elucidate the origin of dissipative processes involved in hydrogels and cells, before applying the relevant poroelastic or viscoelastic theory to model the curves. By using spherical AFM tips, analytical equations were developed to transform these curves into mechanical parameters by describing the relationships between the exerted force and the elastic, poroelastic or viscoelastic responses of semi-infinite and finite-thickness materials. Poroelastic behavior was evidenced for a thermoresponsive hydrogel and a set of poroelastic parameters was extracted from the force relaxation curves. In contrast, cells exhibited viscoelastic properties characterized by a single power-law relaxation over three-decade time scales. In addition, compressive modulus and fluidity exponent of cells were obtained by fitting force relaxation curves and approach-retraction force-distance curves. This combined theoretical and experimental framework opens a rigorous way toward quantitative mechanical properties of soft materials by (1) systematically determining the origin of their relaxation mechanisms, (2) defining the theoretical models to correctly interpret the experimental data, (3) using analytically solved equations to extract the mechanical parameters.

1. Introduction

Atomic force microscopy (AFM) has become an indisputable investigation tool for soft materials and biological samples thanks to its remarkable capability of high-spatial resolution imaging and mapping mechanical properties at the nanoscale, in live conditions and at controlled temperature. In mechanobiology, knowing about the properties of living cells is crucial for deciphering the complex interplay between cells and their physiological state, impacted by external conditions. In the context of tissue engineering, recent studies have precisely established that hydrogels with time-dependent mechanical behaviors significantly enhanced cell proliferation, migration and differentiation, compared to purely elastic hydrogels (Chaudhuri et al., 2020; Lee et al., 2017, 2021). To accurately assess the corresponding rheological properties, various AFM-based methods have been developed by exploiting the piconewton sensitivity in force measurements. However, two main difficulties arise when soft materials are investigated, associated with (1) the experimental procedure to be applied to provide reproducible results and (2) the reliable data analysis to extract quantitative mechanical parameters. Recently, a few studies, bringing together AFM users from different laboratories around the world, have proposed to rationalize the methodology to be followed to measure these properties with reduced artifacts (Schillers et al., 2017; Pérez-Dominguez et al., 2023). Nevertheless, a simple method is still

* Corresponding author.
E-mail address: Stephane.Cuenot@cnrs-imn.fr (S. Cuenot).

https://doi.org/10.1016/j.jmbbm.2024.106865
Received 15 July 2024; Received in revised form 15 November 2024; Accepted 7 December 2024
Available online 9 December 2024

missing combining the determination of theoretical models, that have to be applied to correctly describe the dissipative mechanisms of the probed material, and an analytical processing of the experimental data to extract mechanical properties.

Amongst all AFM-based methods, the most common one consists in acquiring force-distance curves (FDCs), either on a single point of the sample surface or on a whole surface by performing spatially-resolved mapping (*i.e.* force volume). These curves are constructed by recording the force when the tip moves towards the sample surface (approach curve) and withdrawing from the surface (retraction curve). AFM cantilevers with cylindrical, conical (or pyramidal) and parabolic (or spherical) probes are commonly used to perform such force spectroscopy experiments that can directly be carried out on fully hydrated hydrogels or living cells in biological buffers. Since fixing on rigid supports is mandatory, significant overestimations of Young's modulus of soft samples have been reported if their finite-thickness is overlooked due to the stiffer glass or plastic supports (by several orders of magnitude) (Garcia and Garcia, 2018a). To avoid this artefact, bottom-effect corrections have been proposed for FDCs analysis, considering an elastic material with a finite-thickness, indented by probes with various geometries (Garcia and Garcia, 2018b). More recently, several methods have been developed to extract viscoelastic parameters from FDCs by combining bottom-effect correction models and viscoelastic materials. Efremov et al. proposed to numerically calculate the force (F) - indentation (δ) relationship using the Ting's model to describe both the approach and retraction force curves (Efremov et al., 2017). Garcia et al. determined the F-δ equations that can be analytically solved for a conical/pyramidal probe indenting a finite-thickness viscoelastic material by applying the Ting's model and the correspondence principle between elastic and viscoelastic deformations (Garcia et al., 2020).

In the present study, we propose a complete methodology to extract the mechanical parameters for soft materials, especially hydrogels and living cells, by combining AFM indentation and relaxation experiments using spherical AFM tips. Indeed, spherical probes are now more frequently employed thanks to the technical progress in fixing on cantilevers beads or colloids with a wide range of accessible radii, from tens of nanometers to several tens of micrometers, and spring constants spanning over at least four orders of magnitude. In addition, their well-controlled dimensions favor accurate determination of the tip-surface contact geometry requested in contact mechanics models. Firstly, the origin of the dissipative mechanisms involved in the investigated soft materials is determined by analyzing the dependence or not of the force relaxation curves on the tip-surface contact area. Usually omitted, this kind of analyses can elucidate the relevant mechanical models to be applied to the experimental data, such that the time-dependent mechanical properties of soft materials are correctly determined. Differentiating the viscoelastic or poroelastic origin of the dissipative processes involved in hydrogels or living cells is essential to decipher their responses to mechanical stresses. In addition, understanding these dissipative mechanisms is the key step to unravel the structural reorganization of soft materials either by the breaking/reformation of weak crosslinks inducing the rearrangement of their network or the redistribution of solvent through their internal structure. Secondly, analytical expressions relating the force exerted by a spherical tip with the indentation depth are developed as a function of the sample thickness and material properties. Elastic, poroelastic and viscoelastic models are introduced to describe the material properties and used to interpret the experimental force relaxation curves and FDCs. In the future, we suspect that this easy-to-use method could be systematically applied to any soft material to determine its time-dependent mechanical properties from force relaxation curves and FDCs without resorting to complex numerical calculations.

2. Experimental section

2.1. HFF-2 fibroblasts

Human fibroblasts (HFF-2) were purchased from ATCC and cultured in DMEM medium (Gibco) supplemented with 2 mM L-glutamine, 100 IU/mL penicillin, 0.1 mg/mL streptomycin and 10% heat-inactivated fetal calf serum (Gibco). Cells were cultured at 37 °C in a 5% CO_2 atmosphere. Cells were firstly observed by an optical microscope Zeiss Axiovert with a ×10 objective.

To investigate the intracellular organization of HFF-2 cells, the following procedure was applied. All cell lines were seeded at 10 000 cells/well in 200 µL of the appropriate medium in 8 wells IbidiTreat slides and incubated over night at 37 °C in a 5% CO_2 atmosphere to enable the cells to attach to the bottom. After 24h, cells were washed once with PBS and incubated with 1 µg/mL of Wheat Germ Agglutinin Alexa Fluor™ 647 Conjugate (Invitrogen) and 5 µg/mL of Hoechst (Sigma Aldrich) for 30 min at 4 °C to stain the extracellular membrane. In the same way, after 24h, cells were also fixed for 5 min with 4% paraformaldehyde at room temperature in the dark. Cells were washed once with PBS and either incubated with 132 nM of Phalloidin Alexa Fluor™ 647 Conjugate (ThermoFischer Scientific) and 10 µg/mL of Hoechst (Sigma Aldrich) in PBS 0.5% Triton-X100 (Sigma Aldrich) for 1 h at room temperature. The slides were then observed on a Confocal Nikon A1 SIM microscope with a ×60 objective.

2.2. Preparation of pNIPAM-infernan hydrogels

A water-soluble anionic exopolysaccharide (EPS), called infernan, produced by the deep-sea hydrothermal vent bacterium *Alteromonas infernus* (GY785 strain) was used to form a physically crosslinked thermoresponsive hydrogel by grafting with thermosensitive polymer, poly (N-isopropylacrylamide) (pNIPAM) (Fillaudeau et al., 2024). Briefly, the pNIPAM terminal amino groups (-NH_2) (Sigma, Aldrich, Mn 5500 g/mol) reacted with the carboxyl (-COOH) groups of uronic acids of infernan (Mn 900 000 g/mol) through carbodiimide chemistry (EDC/NHS). EPS (20 mg) and pNIPAM-NH_2 (200 mg) were separately dissolved in 1 mL of MES buffer (50 mM, pH 4.8) at room temperature. After overnight solubilization, both solutions were mixed, and EDC (5.9 mg) and NHS (3.6 mg) were added. The reaction mixture was stirred at 250 rpm for 6 h at 20 °C before adding a new EDC/NHS aliquot to favor pNIPAM functionalization with infernan through amidation. After overnight incubation, the product was dialyzed (MWCO 50 000 g/mol) against 0.3 M NaCl (24 h) and Milli-Q water (48 h) and freeze-dried, leading to pNIPAM grafted infernan with 8 % of uronic acid grafted (EPS-p5-8%, Fillaudeau et al., 2024).

2.3. AFM experiments

Prior to AFM measurements, 30 µL of EPS-pNIPAM solution at 10% w/v in PBS 10 mM pH 7.4 were deposited on a Petri dish of 3.5 cm of diameter maintained at 37 °C. After 30 min allowing for gel setting, cell culture medium (DMEM 4.5 g/L glucose) preheated at 37 °C was added. Petri dish glass surface were functionalized with poly-L-lysine (PLL, Sigma). For this purpose, ethanol-washed surface was firstly exposed to UV-ozone treatment for 10 min. Then, 200 µL of PLL at 0.01% were deposited for 30 min. After washing with MilliQ water, the surface was dried. PLL-treated Petri dishes were seeded with 100 000 HFF-2 the day before AFM measurements in 2 mL of the appropriate medium and incubated over night at 37 °C. For the experimentation, 10 mM of HEPES buffer (Sigma-Aldrich) was added to the cultures and Petri dishes were kept at 37 °C during all the acquisition thanks to a thermostat module.

All AFM experiments were performed in liquid environment (HEPES buffer for cells and DMEM for hydrogels) at 37 °C using a NanoWizard II® atomic force microscope (JPK Instruments, Germany) equipped with inverted optical microscope and a temperature controller. Cantilevers

with a glass colloidal sphere of 5 μm in diameter (SQube, Germany) were used for all measurements. Their spring constants, comprised between 0.13 and 0.18 N m^{-1}, were calibrated using the thermal noise method implemented in the AFM setting (JPK software). Prior to mechanical measurements, the cantilever sensitivity was systematically measured from the slope of the force-distance curves performed on a glass substrate. AFM measurements were carried out on two independent EPS-p5-8% hydrogels of ~3 mm thickness, considered as a semi-infinite material because of the low indentation depths. Three fibroblasts were used to acquire force relaxation and FDCs at different locations on their cytoplasmic region. The optical microscope was first used to precisely position the AFM tip on the cytoplasmic region of selected cells by avoiding the nucleus. Then, FDCs were carried out at a low speed of 1 μm s^{-1} to avoid the correction due to hydrodynamic drag forces (F_{drag}) exerted on the cantilever by the liquid medium. The tip-surface contact point in FDC was systematically determined by a double-fitting procedure of the approach curve including a linear fit for the non-contact region and a fit of Hertz model in the contact region (Efremov et al., 2017). The cell height was measured by the difference between the tip-surface contact points of FDCs determined on the cell (at the FDC location) and on the glass substrate (used as a height reference), respectively. The thickness of the investigated cytoplasmic regions varied between around 2 and 6 μm, by considering locations at either the cell edge or the cell center. FDCs were also used to determine the force to be applied with respect to a given indentation depth for the relaxation experiments. Force relaxation curves were recorded on both hydrogels and cells by applying the three-steps procedure as follows: (1) the sample was first indented by the cantilever at high speed (20 μm s^{-1}) until reaching the previously determined depth (approach part), (2) the force relaxation was then measured during 1.5–3 s, while the indentation depth was kept constant (holding phase), (3) the cantilever was eventually retracted from the sample at the same 20 μm s^{-1} speed (retraction part). Force relaxation mapping (20 μm × 20 μm, 32 x 32 pixels) was performed on the cytoplasmic region of HFF-2 fibroblasts with 3 s for the holding phase. All force relaxation curves were corrected by the hydrodynamic drag force to avoid overestimation of extracted parameters, as previously described (Cuenot et al., 2022). As F_{drag} was proportional to the cantilever velocity, only the initial applied force at the initial time was corrected. Interestingly, the force decrease corresponding to the hydrodynamic drag force correction was in the order of a few tenths of nN, similarly to that resulting from time-shift correction, as recently reported (Efremov et al., 2021).

3. Theoretical models

In the following, theoretical models used in this work to analyze both experimental force-distance curves and force relaxation curves are briefly described.

3.1. Models applied to force-distance curves

The models, where a sphere indents either an elastic or a viscoelastic material, are discussed to interpret FDCs. The corresponding equations can be analytically solved to fully describe the approach and retraction parts of experimental FDCs obtained using a spherical AFM tip. In these models, bottom-effect corrections were included to take into account the finite-thickness of soft samples deposited on a solid substrate, thereby avoiding overestimation of the extracted mechanical parameters.

3.1.1. Elastic model for a finite-thickness material

The relation between the applied force (F) and the indentation depth (δ) for a spherical tip (of radius R) into an elastic material characterized by its Young's modulus (or elastic modulus) E and Poisson's ratio ν can be described by the analytical expression (equation (1)):

$$F=\frac{4\sqrt{R}}{3(1-\nu^2)}E\delta^{3/2}\left(1+1.133\frac{\sqrt{R\delta}}{h}+1.497\frac{R\delta}{h^2}+1.469\frac{(R\delta)^{3/2}}{h^3}+0.755\frac{(R\delta)^2}{h^4}\right) \quad (1)$$

where h is the finite-thickness of the elastic sample deposited onto a rigid support (Garcia and Garcia, 2018a). The first term corresponds to the Hertz model for a semi-infinite elastic material, independent on h. The additional terms in polynomial series of $((R\delta)^{1/2}/h)^n$ represent the bottom-effect corrections yielding the elastic modulus of the investigated material without overestimation due to the rigid support.

3.1.2. Viscoelastic model for a finite-thickness material

For the approach part of the force curves, where the contact area increases monotonically with time, the elastic-viscoelastic correspondence principle developed by Lee and Radok can be applied to determine the dependence of the force with indentation and time (t) (Lee and Radok, 1960). The force exerted by a rigid spherical probe on a linear viscoelastic material can then be expressed as (equation (2)):

$$F(t,\delta(t))=\sum_{i=0}^{N}\alpha_i\int_0^t\Psi(t-\tau)\frac{d\delta(\tau)^{\beta_i}}{d\tau}d\tau \quad (2)$$

where the coefficients α_i and β_i incorporate the bottom-effect viscoelastic corrections for the finite-thickness sample and $\Psi(t)$ is the relaxation function describing the material viscoelasticity (Garcia and Garcia, 2018b). Amongst the various viscoelastic models, the relaxation function corresponding to the power-law rheology (PLR) model takes the following form (equation (3)):

$$\Psi_{PLR}(t)=E_0\left(\frac{t}{t_S}\right)^{-\alpha} \quad (3)$$

where E_0 is defined as the compressive modulus of the material at time t_S (a timescale factor usually set to 1 s) and α is the fluidity exponent (Kollmannsberger and Fabry, 2011). This exponent characterizes the dissipative effects with a 0 value for an elastic solid while a 1 value describes a viscous (Newtonian) liquid. The force exerted on a viscoelastic material defined by the PLR relaxation function can be calculated by integrating equation (3) into equation (2) (equation (4)):

$$\begin{aligned}F_{app}=&\frac{4\sqrt{R}}{3(1-\nu^2)}E_0\left(\frac{t}{t_S}\right)^{-\alpha}\delta^{3/2}\\&\left(\frac{3}{2}\frac{\Gamma\left(\frac{3}{2}\right)\Gamma(1-\alpha)}{\Gamma\left(\frac{5}{2}-\alpha\right)}+1.133\frac{\sqrt{R\delta}}{h}2\frac{\Gamma(2)\Gamma(1-\alpha)}{\Gamma(3-\alpha)}\right.\\&+1.497\frac{R\delta}{h^2}\frac{5}{2}\frac{\Gamma\left(\frac{5}{2}\right)\Gamma(1-\alpha)}{\Gamma\left(\frac{7}{2}-\alpha\right)}+1.469\frac{(R\delta)^{3/2}}{h^3}3\frac{\Gamma(3)\Gamma(1-\alpha)}{\Gamma(4-\alpha)}\\&\left.+0.755\frac{(R\delta)^2}{h^4}\frac{9}{2}\frac{\Gamma\left(\frac{9}{2}\right)\Gamma(1-\alpha)}{\Gamma\left(\frac{11}{2}-\alpha\right)}\right)\end{aligned} \quad (4)$$

where Γ is the gamma function. This analytical expression, only valid for the approach FDCs, incorporates bottom-effect corrections where the first term, independent on h, corresponds to the force exerted by the spherical tip on a semi-infinite PLR sample. Additional terms are included to take into account the finite-thickness of the viscoelastic sample.

During the tip's withdrawal from the sample (retraction part of force curves), Lee-Radok's theory is no longer valid since the contact area does not increase anymore monotonically (Lee and Radok, 1960). To overcome this limitation, the Ting's method is usually used to determine the force applied to a viscoelastic material during the retraction curve

(Ting, 1966). The basic idea of this method is that a given time in the retraction curve (t, $t > t_{max}$ where t_{max} is the time corresponding to the maximum indentation depth) corresponds to an equivalent time $t_1(t)$ in the approach curve ($0 < t_1 < t_{max}$) with the same contact area. The force corresponding to the retraction curve can then be obtained by integrating equation (2) from 0 to $t_1(t)$, instead of 0 to t. The expression of $t_1(t)$ in function of t has to be previously determined by solving equation (5):

$$\int_{t_1(t)}^{t} \Psi(t-\tau)\frac{d\delta(\tau)}{d\tau}d\tau = 0 \tag{5}$$

The analytical expression of $t_1(t)$, calculated for the PLR relaxation function (equation (3)) by assuming a triangular ramp of indentation with time, is written as follows (equation (6)):

$$t_1(t) = t - \sqrt[1-\alpha]{2}(t - t_{max}) \tag{6}$$

The F-δ relation, valid for the retraction FDCs, can be analytically solved by including equation (6) into equation (2) (equation (7)):

$$F_{ret} = \frac{4\sqrt{R}}{3(1-\nu^2)}E_0\left(\frac{t_1}{t_S}\right)^{-\alpha}\delta^{3/2}\left(\frac{3}{2}\frac{\Gamma\left(\frac{3}{2}\right)\Gamma(1-\alpha)}{\Gamma\left(\frac{5}{2}-\alpha\right)} + 1.133\frac{\sqrt{R\delta}}{h}2\right.$$
$$\frac{\Gamma(2)\Gamma(1-\alpha)}{\Gamma(3-\alpha)} + 1.497\frac{R\delta}{h^2}\frac{5}{2}\frac{\Gamma\left(\frac{5}{2}\right)\Gamma(1-\alpha)}{\Gamma\left(\frac{7}{2}-\alpha\right)} + 1.469\frac{(R\delta)^{3/2}}{h^3}3 \tag{7}$$
$$\left.\frac{\Gamma(3)\Gamma(1-\alpha)}{\Gamma(4-\alpha)} + 0.755\frac{(R\delta)^2}{h^4}\frac{9}{2}\frac{\Gamma\left(\frac{9}{2}\right)\Gamma(1-\alpha)}{\Gamma\left(\frac{11}{2}-\alpha\right)}\right)$$

Other viscoelastic models can be chosen for describing the viscoelastic character of the probed material through the relaxation function (Bonfanti et al., 2020). The Kelvin-Voigt model corresponding to the combination of a spring (elastic element) and a dashpot (viscous element) in parallel also leads to analytical approach-retraction expressions. However, a step discontinuity systematically occurs between calculated approach and retraction FDCs due to the change in the sign of the velocity when FDCs are generated by using a triangular waveform (Sanchez et al., 2021). In this case, the resulting analytical expressions of the Kelvin-Voigt model cannot be used to fit the experimental approach-retraction FDCs. All the other viscoelastic models conduct to non-analytical expressions requiring numerical calculations to interpret both approach and retraction FDCs in the case of indentation experiments using a triangular waveform and spherical AFM tips.

3.2. Models applied to force relaxation curves

Force relaxation curves can be analytically described using either viscoelastic or poroelastic models depending on the material behavior.

3.2.1. Viscoelastic model for a finite-thickness material

In the case of a viscoelastic material, the force relaxation expression can be calculated from equation (1) by replacing the Young's modulus E with an expression of the elastic relaxation modulus $E(t)$. Various $E(t)$ functions corresponding to different viscoelastic models could be incorporated into equation (1). In this study, PLR model was investigated by including equation (3) into equation (1), to give the force relaxation expression for a finite-thickness PLR sample. Another expression of $E(t)$ was tried to analyze relaxation curves with the generalized Maxwell model (several Maxwell elements in parallel, each composed of an elastic spring and a viscous damper in series) developed here with two relaxation times (τ_1, τ_2) as defined by equation (8).

$$E(t) = E_\infty + E_1\, exp(-t/\tau_1) + E_2\, exp(-t/\tau_2) \tag{8}$$

where E_∞ is the long-time elastic modulus, and E_1, E_2, the elastic components relative to the relaxation processes characterized by τ_1, τ_2, respectively.

3.2.2. Poroelastic theory

Based on the original theory developed by Biot, Tanaka et al. have formulated the poroelastic theory usually applied to macroscopic measurements on hydrogels and cells (Biot, 1956; Tanaka et al., 1973). This theory was used to correctly interpret force relaxation experiments measured by keeping constant the indentation depth of an indenter of different geometries (*e.g.* cylinder, sphere …) and sizes (from millimeter to nanometer) (Hu et al., 2010). However, there is no analytical solution relating force and time for a poroelastic material indented by a sphere. From finite-element simulations, Hu et al. have proposed an analytical expression to describe the normalized relaxation curves in response to an indentation by a spherical probe (Hu et al., 2010) (equation (9)):

$$\frac{F(t)-F_\infty}{F_0-F_\infty} = 0.491\, exp\left(-0.908\sqrt{\theta}\right) + 0.509\, exp(-1.679\theta) \tag{9}$$

where θ corresponds to the measured time normalized by the poroelastic time τ_P, which is defined by the ratio between the tip-surface contact radius (a) and the poroelastic diffusion coefficient (D) (Lin and Hu, 2006) (equation (10)):

$$\tau_P = \frac{a^2}{D} \tag{10}$$

The tip-surface contact radius is commonly determined using the Hertz contact theory for a spherical indenter of radius R penetrating an elastic material at a depth δ by (Hertz, 1881) (equation (11)):

$$a = \sqrt{R\delta} \tag{11}$$

To apply equation (9) to experimental force relaxation curves, all curves were normalized using $(F - F_\infty)/(F_0 - F_\infty)$, where F_0 corresponds to the instantaneous force response and F_∞ is the constant force reached at equilibrium (Hu et al., 2010). When the solvent drainage is negligible due to fast enough indentation, the Poisson's ratio ν_∞ at equilibrium of the porous network is determined from forces at short and long time scales, as follows (Hu et al., 2010) (equation (12)):

$$\frac{F_0}{F_\infty} = 2(1-\upsilon_\infty) \tag{12}$$

Using the instantaneous force response, the elastic modulus of the poroelastic material can be calculated by considering it as incompressible at the initial time (Hu et al., 2010) (equation (13)):

$$E = \frac{9}{16}\frac{F_0}{\delta_0^{3/2}R^{1/2}} \tag{13}$$

The permeability κ of the poroelastic material can then be estimated knowing the previously determined parameters D, ν_∞ and E (Moeendarbary et al., 2013) (equation (14)):

$$\mathrm{K} = \frac{D\eta}{E}\frac{(1+\upsilon_\infty)(1-2\upsilon_\infty)}{(1-\upsilon_\infty)} \tag{14}$$

where η is the solvent viscosity at the experimental temperature.

4. Results and discussion

Various AFM-based methods have been developed to probe the mechanical properties of soft samples by operating either in time (FDCs, force relaxation or creep relaxation …) or in frequency domain (force modulation, resonance frequency measurement …) (Cuenot et al., 2008; Hecht et al., 2015; Moreno-Guerra et al., 2019). In time domain, the most common method to investigate the mechanical properties of soft materials is to record conventional FDCs where the applied force is

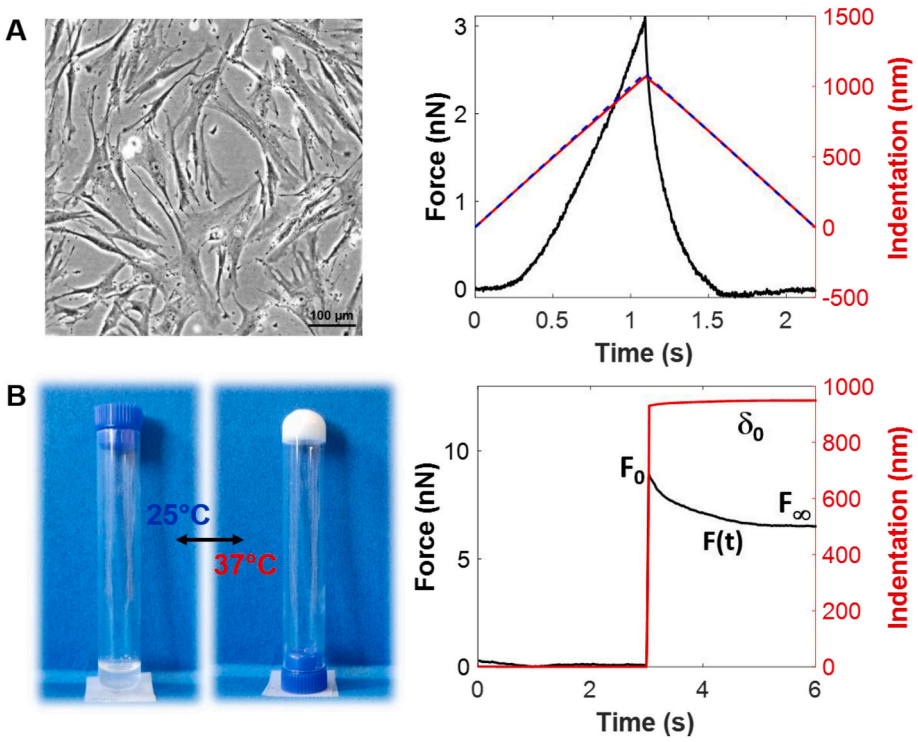

Fig. 1. (A) Optical microscopy image of human fibroblast (HFF-2) cells, experimental force-time and indentation-time data recorded on the cytoplasmic region of HFF-2 cells in HEPES buffer at 37 °C by applying a maximum force of 3 nN (corresponding to an indentation depth of ~1000 nm) at 1 µm s^{-1}. The blue dashed line corresponds to the indentation depth calculated using equation (15). (B) Pictures showing the thermoresponsive character of pNIPAM-grafted-infernan hydrogel with a liquid state at 25 °C and a gelled state at 37 °C. Force relaxation curve measured on pNIPAM-grafted-infernan hydrogel in DMEM at 37 °C during the holding phase of 3 s while the indentation depth was kept constant at ~950 nm.

measured as a function of indentation or time. Fig. 1A shows in a conventional FDC, the experimental dependence of the force with time obtained on cell surface using a triangular waveform for indentation with time.

For this indentation ramp, the indentation depth can easily be calculated as a function of time by decomposing it into two parts (approach part for $t \leq t_{max}$ and retraction part for $t > t_{max}$):

$$\delta(t) = \begin{cases} vt, t \leq t_{max} \\ v(2t_{max} - t), t > t_{max} \end{cases} \quad (15)$$

where t_{max} is the time corresponding to the maximum indentation depth and v the cantilever velocity (Sanchez et al., 2021). The experimental dependence of indentation depth with time was well described by equation (15) (Fig. 1A), enabling calculations of the contact time of the tip within the materials. Mechanical responses of hydrogels or cells are strongly dependent on the tip velocity used in the experiment or the modulation frequency, which is related to the contact time (Rigato et al., 2017). Indeed, the corresponding frequency is obtained by the inverse of the contact time (Sanchez et al., 2021). Here, contact times of the tip within hydrogels or cells, comprised between 1.3 s and 2.4 s according to the indentation depth, imply frequencies in the range of 0.4–0.8 Hz.

Another interesting method to access the time-dependent mechanical properties of soft samples is to perform force (or stress) relaxation experiments. In these experiments, a high constant speed is used to vertically approach the cantilever to the sample surface before increasing force and indentation until reaching a predefined indentation depth δ_0 (Fig. 1B). The force decay is then measured as a function of time, defining the force relaxation curve $F(t)$, while the indentation depth is kept constant at δ_0. The instantaneous force response F_0 is thus measured at the initial time t_0 when the indentation depth reached δ_0, and F_∞ is the force reached at the equilibrium state. Contrary to a creep experiment, both force and tip-surface contact radius decrease with time during this holding phase. The obtained force relaxation curve corresponds to a modified force curve where a holding phase is added between the conventional approach and retraction parts.

4.1. Poroelastic or viscoelastic responses

Spherical AFM tips with beads or colloids are widely used to investigate the mechanical properties of soft materials, notably due to their well-defined radius of curvature favoring the accurate determination of the tip-surface contact geometry needed in the contact mechanics models. Another interesting advantage of using colloidal tips is the reduction in stress concentration at its edges compared to other shapes like cylinder or cone. When hydrogels and living cells are compressed or indented by an AFM tip, their time-dependent mechanical responses arise from either the solvent movement and redistribution through their internal structure (*i.e.* poroelasticity) or the reformation of crosslinks and rearrangement of their network (*i.e.* viscoelasticity) (Hu et al., 2010). These two distinct behaviors have to be differentiated to correctly analyze the experimental data with the appropriate poroelastic or viscoelastic models. However, this essential step is usually neglected and viscoelastic models are used as default, which may lead to incorrect mechanical parameters extracted when inappropriate theoretical models are applied. Indeed, some studies have reported opposite behaviors for cells, with poroelasticity being responsible for the energy dissipation involved in their time-dependent mechanical responses in some cases, while relaxation mechanisms originated from viscoelasticity for the others (Moeendarbary et al., 2013; Hecht et al., 2015; Wei et al., 2016; Efremov et al., 2017; Sanchez et al., 2021). No general consensus could be revealed, notably because of the wide variety of characteristic lengths, such as the tip-surface contact diameters, and time scales explored in AFM experiments. In addition, the complex time-dependent mechanical properties of living cells and tissues may involve poro-viscoelastic properties where poroelasticity and viscoelasticity compete

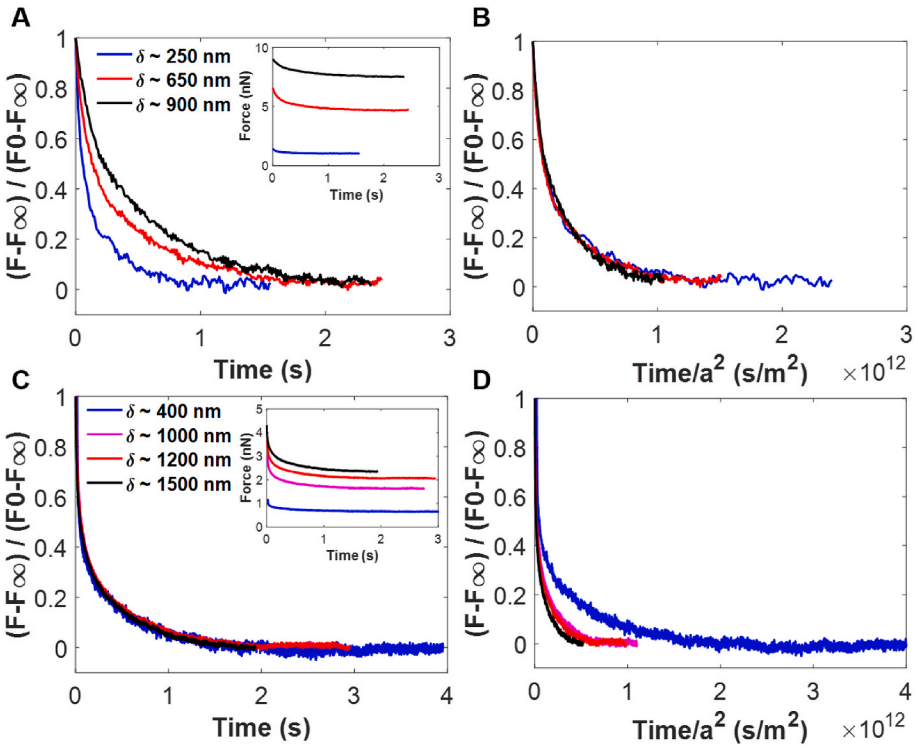

Fig. 2. (A) Force normalization of force relaxation curves measured in a pNIPAM-grafted-infernan hydrogel for three indentation depths, δ (raw data in the inset). (B) Superimposition of force relaxation curves after force and time normalizations revealing the poroelastic behavior of pNIPAM-grafted-infernan hydrogel. (C) Superimposition of force relaxation curves after force normalization measured on the cytoplasmic region of fibroblast cells revealing their viscoelastic behavior (raw data in the inset for four indentation depths). (D) Force relaxation curves after force and time normalizations.

(Moeendarbary et al., 2013). These two mechanisms can dominate at different time scales as already evidenced with poroelastic relaxations at short times and viscoelastic responses at longer times (Moeendarbary et al., 2013). Therefore, systematic determination of dissipation mechanisms involved in the time-dependent mechanical properties should be carried out in relation to the experimental conditions.

Poroelasticity and viscoelasticity can easily be distinguished by exploiting the strong dependence of poroelastic properties with the tip-surface contact size, while viscoelastic properties are size-independent. In this way, force relaxation curves may be recorded at different indentation depths to vary the tip-surface contact size (Hu et al., 2010; Cuenot et al., 2022). Fig. 2A shows three experimental force relaxation curves measured at different indentation depths (between 250 nm and 900 nm) in the pNIPAM-grafted-infernan hydrogel until an equilibrium state was reached after ~2 s. The diameter of the tip-surface contact area, calculated from the Hertz contact theory using equation (11), varied for these indentation depths between 1.6 μm (δ_0 = 250 nm) and 3.0 μm (δ_0 = 900 nm) (Hertz, 1881). These raw relaxation curves were normalized using $(F - F_\infty)/(F_0 - F_\infty)$, where F_0 corresponds to the instantaneous force response measured at t_0 and F_∞ is the force reached at the equilibrium state (Hu et al., 2010). The normalized curves did not superimpose into a single one, thus revealing their dependence with the tip-surface contact size. This poroelastic behavior was also confirmed by the increase of the relaxation with the indentation depth (*i.e.* the contact size) indicating that slower relaxation corresponded to a longer transport of solvent molecules through the hydrogel network, and conversely (Fig. 2A). After additional normalization of the time by the tip-surface contact area (*i.e.* a^2), the three normalized curves collapsed into a master curve confirming that the poroelastic relaxation was proportional to the size of the deformed network by the AFM tip (Fig. 2B). Surprisingly, the thermoresponsive pNIPAM-grafted-infernan hydrogel exhibited a poroelastic behavior, while a physically crosslinked hydrogel obtained by mixing unmodified infernan with calcium was recently shown to be viscoelastic (Cuenot et al., 2022). Contrary to chemically (covalently) crosslinked hydrogels possessing poroelastic properties, distinct mechanisms govern the time-dependent mechanical properties of physically (non-covalent) crosslinked hydrogels as a function of the nature of the crosslinked networks (Zhao et al., 2010; Lee et al., 2016; Cuenot et al., 2022). Indeed, in the case of weak ionic crosslinks, formed in infernan/calcium hydrogels, their disruption and reformation in response to the force applied by the AFM tip conducted to the viscoelastic dissipation of mechanical stresses (Makshakova et al., 2022; Zykwinska et al., 2022; Cuenot et al., 2022). For the investigated EPS-pNIPAM polymer, hydrophobic interactions between pNIPAM chains grafted on the polysaccharide backbone led to gel formation at 37 °C (*i.e* above the lower critical solution temperature of pNIPAM). In this thermoresponsive hydrogel, poroelastic relaxation through solvent migration was favored, while keeping intact the crosslinked network. Such a poroelastic behavior was already evidenced for other pNIPAM-based hydrogels (Yoon et al., 2010; Delavoipière et al., 2016). In the following, the poroelastic thermoresponsive hydrogel was considered as a biphasic material consisting of a porous elastic network immersed in an interstitial fluid.

This straightforward method was applied to the cytoplasmic region of fibroblast cells to investigate the origin of their dissipative mechanisms. Indeed, the cytoplasm mainly dictates the time-dependent mechanical properties of cells because of its greater contribution to cell volume and its rate associated with deformations of cell shape. Prior to AFM measurements, the optical microscope was used to position the AFM tip on the selected region of the cell. Force relaxation experiments were performed at different indentation depths comprised between 400 and 1500 nm. Fig. 2C shows the superimposition of four force relaxation curves into a single curve after normalizing the measured forces. These results clearly reveal that the relaxation mechanisms of fibroblast cells were independent on the contact size (diameters varying between 2 and 4 μm). The time-dependent mechanical responses of cells, after

compression by a spherical AFM tip, originated from their viscoelastic properties and not from poroelastic relaxation. Their viscoelastic character was also confirmed by the non-superimposition of the curves after further normalization of time by the tip-surface contact area (Fig. 2D). In addition, the evolution of relaxation with the indentation depth is opposite to that previously observed for the poroelastic behavior of thermoresponsive hydrogel. Indeed, slower relaxations for lower indentation depths constitute another signature of the observed viscoelastic behavior (Wei et al., 2016; Cuenot et al., 2022).

Finally, from simple force relaxation curves measured at different indentation depths, the dependence or not of normalized curves (after force normalization) with the tip-surface contact size clearly revealed the poroelastic or viscoelastic character of the time-dependent mechanical properties of soft materials, like hydrogels and cells.

In the following, poroelastic theory has to be applied to analyze the experimental data measured on pNIPAM-grafted-infernan hydrogels to correctly determine their time-dependent mechanical properties. In this case, the use of viscoelastic models is clearly inappropriate and would lead to wrong interpretation of their mechanical properties. An opposite result was obtained for fibroblast cells for which viscoelastic models have to be considered to describe their temporal mechanical responses. This difference in relaxation behaviors results from the microstructural differences between hydrogels and cells. Indeed, the more porous network of hydrogels with relatively uniform pore size favors more easily the motion of solvent molecules and their redistribution through the network during mechanical compression. In contrast, cells possess a cytoskeletal network composed of microtubules and (actin and intermediate) filaments, and a cytoplasm constituted of organelles and various macromolecules bathed in cytosol. Under AFM tip deformation, this more complex and disordered structure (*e.g.* larger pore size variation) induces the reorganization of the cytoskeletal network and reformation of weak crosslinks between polymeric chains.

4.2. Poroelastic properties of hydrogels

Based on the original theory developed by Biot, Tanaka et al. have formulated the poroelastic theory usually applied to macroscopic measurements on hydrogels and cells (Biot, 1956; Tanaka et al., 1973). This theory was used to correctly interpret force relaxation experiments performed with spherical indenters of different sizes including AFM tips (Chan et al., 2012; Moeendarbary et al., 2013). Several independent parameters characterizing the mechanical properties of poroelastic material were quantified from the experimental force relaxation curves. These curves can easily be fitted by the equation proposed by Hu et al. with a single adjustable parameter, the diffusion coefficient D, and known parameters F_0, F_∞ and a^2 (equation (9)) (Hu et al., 2010). In Fig. 3A, a good agreement was obtained between three experimental curves and the poroelastic equation of Hu with the diffusion coefficient values of 4.6 (indentation depth of 250 nm), 4.9 (650 nm), and 4.8 μm^2 s^{-1} (900 nm). Interestingly, these poroelastic diffusion constants were found to be very similar and independent from the indentation depth, indicating that the network structure of the hydrogel was homogeneous. These three experimental force relaxation curves, normalized both in force and in time by the poroelastic time τ_P, were remarkably superimposed in the range of experimental times, while the normalized time was represented in logarithmic scale (Fig. 3B). In addition, the universal curve proposed by Hu (equation (9)) perfectly matches with the experimental data (without any fitting parameter) confirming that hydrogels behave as purely poroelastic materials, without exhibiting complex poroviscoelastic properties in the investigated experimental conditions.

All the measured values for the diffusion coefficient of water in pNIPAM-grafted-infernan hydrogels were gathered in a boxplot representation with a mean value of 3.3 ± 1.1 μm^2 s^{-1} (mean ± standard deviation) (Fig. 3C). Larger D values corresponded to faster relaxations and lower associated relaxation times. In the investigated hydrogels, relaxation results from water molecules moving out of the compressed

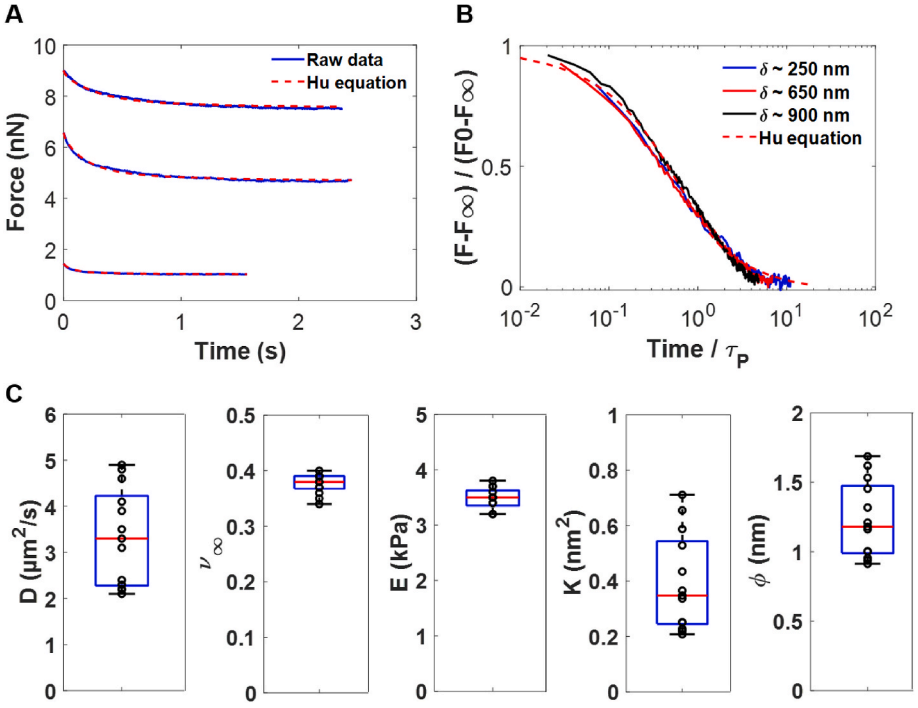

Fig. 3. (A) Superimposition of experimental force relaxation curves measured on the pNIPAM-grafted-infernan hydrogel and fitted curves with the Hu's equation (the diffusion coefficient D as the single adjustable parameter) for three indentation depths (250 nm, 650 nm and 900 nm). (B) Superimposition of force relaxation curves in semi-log plot after both force normalization and time normalization by the poroelastic time τ_P, in agreement with the universal curve proposed by Hu. (C) Boxplot representation of the poroelastic diffusion coefficient (D) values, Poisson's ratio (ν_∞) values, elastic modulus (E) values, permeability (K) values and the pore size (ϕ) values of the poroelastic hydrogel.

region by the AFM tip. To confirm that the poroelastic properties of hydrogels are well probed, it is essential to check that the poroelastic time (τ_P) associated with this relaxation is much longer than the time needed to reach the indentation depth (experimental rise time τ_R). Time τ_R ~50 ms for an indentation of 1 μm was measured, while τ_P ~750 ms was obtained using equation (10), meaning that water displacement inside the porous network of hydrogels was effectively responsible for the measured relaxation. Using a high cantilever velocity (20 μm s^{-1}) for the approach part of the relaxation experiments, the undrained condition was respected, indicating that the interstitial fluid cannot drain out of the compressed region by the AFM tip, at short times. Conversely for longer times, water was redistributed within the porous network and F_∞, divided by the tip-surface area, was at the equilibrium state with the elastic stress due to the porous network, only. The Poisson's ratio ν_∞ at equilibrium of the porous matrix was determined from forces at short and long-time scales with a mean value of 0.38 ± 0.02 (Fig. 3C) (equation (12)). These values were in excellent agreement with those published for other polyacrylamide-based poroelastic hydrogels (Yoon et al., 2010; Berry et al., 2020). For a given indentation depth, the elastic modulus of the poroelastic hydrogel was calculated using the instantaneous force response (equation (13)). A mean value of 3.5 ± 0.2 kPa was obtained, in good agreement with those previously measured for another physically crosslinked hydrogels based on infernan. Indeed, elastic modulus values comprised between 3 and 8 kPa were measured depending on infernan and calcium concentrations (Cuenot et al., 2022; Zykwinska et al., 2022). The permeability of the poroelastic pNIPAM-grafted-infernan hydrogels was then estimated to be 0.4 ± 0.2 nm^2 (equation (14)), using previously determined parameters D, ν_∞, E, and solvent (DMEM) viscosity (0.73 mPa s at 37 °C) (Poon, 2022). From this permeability value, an approximate pore size of the hydrogel network was estimated to be 1.3 ± 0.3 nm, determined according to the study of Chan et al. (2012). Pore diameters in the range of 1–10 nm have been reported in the literature for pNIPAM-based hydrogels, depending both on the used measurement technique and the heterogeneity of the structure in relation with the synthesis conditions (Yoon et al., 2010; Berry et al., 2020). The obtained pore size was considerably lower than the tip radius of 2.5 μm, meaning that the mechanical responses probed by the AFM tip actually come from the composite material consisting of the hydrogel hydrated network and the solvent passing through the nanopores.

4.3. Viscoelastic properties of fibroblast cells

Contrary to poroelastic properties that were extracted from force relaxation measurements, viscoelastic properties can be determined from either force-distance curves or force relaxation curves. In time domain, FDC measurement is by far the most commonly used method to probe mechanical properties of soft materials but their transformation into quantitative viscoelastic parameters such as the elastic modulus at the equilibrium state, relaxation times, or fluidity exponent remains a complex task. In the context of mechanical analyses of cells, power-law based-models have widely been used to describe the cell response to an external force (Moeendarbary et al., 2013; Hecht et al., 2015). In particular, the PLR model has been successfully applied to cells using an analytical expression to fit FDC recorded with pyramidal AFM tips or by requiring numerical calculations for others tip shapes (Efremov et al., 2017; Sanchez et al., 2021). Here, in the case of experiments conducted with spherical AFM tips, the developed analytical equations (equations (4) and (7)) were used to fit both approach and retraction parts of experimental FDCs with the PLR model by the least-squares method (Fig. 4A). The excellent agreement obtained with only two adjustable parameters, the compressive modulus E_0 and the fluidity exponent α, fully validated the use of the PLR model to describe the viscoelastic properties of fibroblasts. This calculation was performed by considering the tip-surface contact mechanics, the deformation history (*via* the Ting's method) and the finite-thickness of cells to avoid overestimation of mechanical properties by the rigid substrate.

All values of E_0 and α extracted from FDCs were reported in the boxplot representation by modelling the investigated cells either as a semi-infinite viscoelastic material or as a finite-thickness viscoelastic material (*i.e.* without or with bottom-effect corrections) (Fig. 4B). Mean values of compressive modulus were found to be equal to 2.5 ± 0.9 kPa by considering the semi-infinite model and 2.1 ± 0.7 kPa for the finite-thickness cell. As expected, overestimating E_0 due to the glass support was revealed for the semi-infinite model, while the fluidity exponent remained unaffected (values comprised between 0.1 and 0.4 with a mean value of 0.2 ± 0.1). The range of E_0 values was comprised between 1.3 kPa and 4.0 kPa by analyzing curves with the semi-infinite viscoelastic model and between 1.1 kPa and 3.5 kPa by considering the cell thickness. These dispersed values, measured on the cytoplasmic region of three HFF-2 fibroblast cells, reflected both the complexity and the high heterogeneous character of their structure. Fig. 5 shows the heterogeneity of cells in terms of the dispersion of intracellular vesicles, the position of the nucleus and the actin cytoskeleton. This could contribute to the difference between AFM measurements depending on the position of the tip on the cell surface. In addition, differences between cells exist due to their non-synchronization in the cell cycle with different states of progress, which will have consequences on the structuring of the actin network. The obtained values of E_0 and α parameters are close to those already published for other fibroblast cells (namely NIH 3T3) after FDC measurements (Sanchez et al., 2021). Sanchez et al. revealed a similar trend for the dependence of these parameters on the rigid support, after analyzing FDCs performed on the cytoplasmic region of NIH 3T3 fibroblast cells with pyramidal tips (Sanchez et al., 2021). In addition to these viscoelastic properties, the elastic components of cells can be determined by fitting equation (1) (through its single adjustable

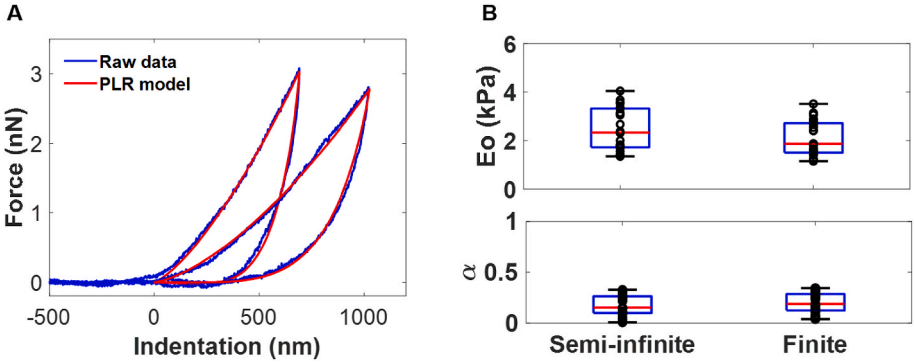

Fig. 4. (A) Superimposition of experimental force-indentation curves measured on the cytoplasmic region of HFF-2 fibroblast cells and fitted curves with the analytical power-law rheology model by the least-squares method. PLR parameters: E_0 3.5 kPa, α 0.35 (left curve), E_0 1.2 kPa, α 0.25 (right curve). (B) Influence of the rigid support on E_0 and α values of the PLR model by using an infinite thickness for cells (semi-infinite model) or the measured thickness (finite-thickness model).

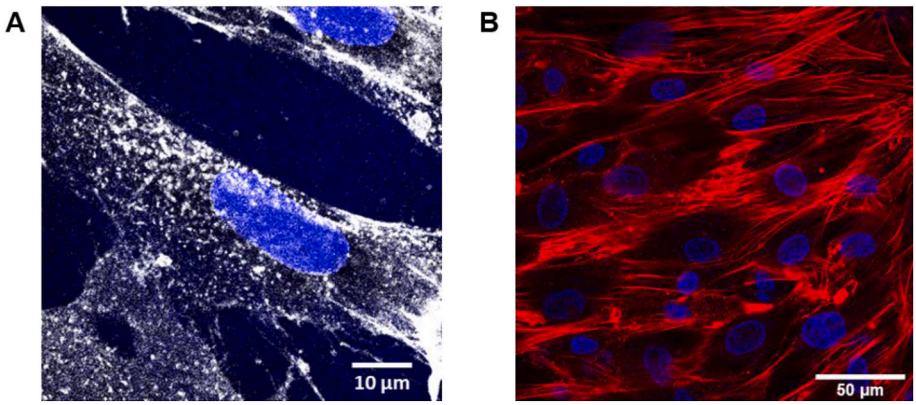

Fig. 5. Intracellular organization of HFF-2 cells. (A) Cells were labelled with Wheat Germ Agglutinin Alexa Fluor™ 647 Conjugate to stain the cellular membranes: white, WGA; blue, nuclei. (B) Cells were labelled with Phalloidin-647 Conjugate to stain actin network: red, phalloidin; blue, nuclei. Cells were observed on a Confocal Nikon A1 RS microscope with a ×60 objective.

parameter, the elastic modulus) for the approach FDC, by taking into account or not the cell height (see Supplementary Information).

Another interesting approach to determine the viscoelastic properties of soft materials is to analyze the force relaxation curves. Indeed, different viscoelastic models can be applied to describe the relaxation of the measured force by including either exponential laws or power laws. Among these models, the generalized Maxwell model, where several Maxwell elements composed by a spring (elastic) and a dashpot (viscous) in series are connected in parallel, is frequently applied to determine relaxation times associated with relaxation processes (equation (8)). However, this model was unable to correctly describe the obtained experimental decays, no matter which exponential law (mono- or double) was considered (see Supplementary Information). Therefore, the viscoelastic relaxation of cells subjected to AFM indentation does not follow a single or double decreasing exponential law.

The PLR model that correctly describes the viscoelastic response of HFF-2 fibroblast cells to the force applied by spherical AFM tips, as revealed in Fig. 4A, can also be applied to force relaxation curves. In this case, the elastic modulus used in the elastic model (equation (1)) was replaced with the elastic relaxation modulus $E(t)$ defined by the expression of the PLR model (equation (3)), giving then the force relaxation expression for a finite-thickness PLR sample. Fig. 6A shows three experimental force relaxation curves, measured for an indentation depth of about 1 µm, fitted with the PLR model by adjusting its two parameters, E_0 and α, by the least-squares method. To assess the quality of the fits and confirm that the experimental curves follow a power-law decay, it is worth plotting them with a log-log scale. In this representation, all curves were transformed into straight lines with a single slope, showing no crossover over the experimental three-decade time ranges from 1 ms to 3 s (Fig. 6B). This result indicates that only one mechanism was at the origin of time-dependent mechanical responses of cells under the used experimental conditions. Combined with the viscoelastic

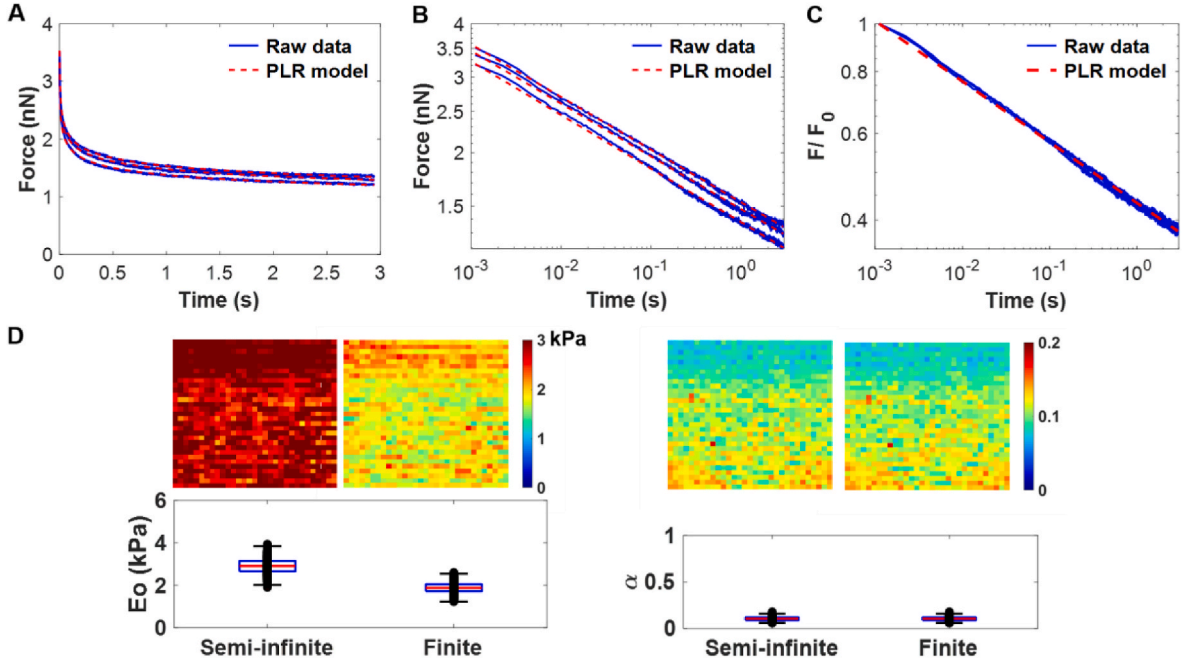

Fig. 6. (A) Three experimental force relaxation curves and theoretical curves obtained by adjusting the two parameters of the power-law rheology model by the least-squares method. (B) Log-log representation of experimental curves and fitted curves by the PLR model. (C) Normalized plots of F/F_0 as a function of time in log-log representation, where F_0 is the force at the initial time. (D) Mapping of the PLR model parameters (Eo, α) and boxplot representation of the obtained values from the force relaxation mapping (20 µm × 20 µm, 32 × 32 pixels) performed on the cytoplasmic region of HFF-2 fibroblast cell. Data analysis was performed by considering the cell height either as infinite (semi-infinite model) or as measured (finite-thickness model).

character evidenced in Fig. 2C, only viscoelasticity and not poro-viscoelasticity governs the relaxation behavior observed at multiple time scales. In addition, theoretical curves of the PLR model perfectly match the experimental ones, confirming the correct use of this model to describe the mechanical response of fibroblast cells, as previously discussed from FDC analysis (Fig. 4A). Normalizing all these curves by F_0 led to a master straight line of slope 0.13, corresponding to the power-law exponent α (Fig. 6C). Finally, the relaxation behavior of fibroblast cells resulting from a micron-scale indentation was accurately described over three-decade time scales by a single power-law viscoelastic model.

To generate spatially-resolved maps of mechanical properties, force-volume experiment is widely used to record FDC on each point of the surface prior to their individual analysis resorting to theoretical models (Cuenot et al., 2017; Sanchez et al., 2021). In Fig. 6D, an original alternative was proposed by performing a force relaxation mapping of a 20 μm × 20 μm area located on the cytoplasmic region of HFF-2 fibroblast cell with acquisition of 32 × 32 force relaxation curves (Hecht et al., 2015). After fitting every curve with the PLR model, with or without considering the finite-thickness of cells, two maps of E_0 and α were constructed by plotting these parameters as a function of their spatial coordinates. Values of E_0 were clearly affected by the rigid support with higher values in the case of semi-infinite model (comprised between 1.9 and 3.9 kPa with a mean value of 2.9 ± 0.4 kPa) compared to those obtained by considering the local cell thickness (between 1.2 and 2.6 kPa with a mean value of 1.9 ± 0.3 kPa). All these compressive modulus values were found to be very close to those extracted from FDC measurements, emphasizing the consistency of the obtained results by two different methods. In the same way, α values were completely independent on the cell thickness, as previously observed from the analysis of FDC. These values, comprised between 0.06 and 0.23, were slightly lower than those deduced from FDC analysis, but in the range of published values (Efremov et al., 2017; Sanchez et al., 2021). Maps of PLR parameters revealed two distinct regions (although the spatial resolution was not the aim of this force relaxation mapping) where higher E_0 values corresponded to lower α values for the more solid-like region, and inversely for the more fluid-like region.

5. Conclusions

In this work, AFM-based force relaxation curves were firstly measured to determine the origin of energy dissipation mechanisms taking place in hydrogels and cells during their compression. Two different behaviors were clearly evidenced with the mechanical responses proportional to the tip-surface contact size for thermoresponsive physical hydrogels, while those measured on the cytoplasmic region of fibroblast cells were size-independent. Based on this assessment, two distinct theories have to be applied to correctly analyze the experimental data with poroelastic models for these hydrogels and viscoelastic ones for fibroblast cells. Poroelastic parameters, including elastic modulus, Poisson's ratio as well as transport properties like the solvent diffusion coefficient through the nanoporous network, were then estimated by fitting experimental force relaxation curves. Regarding viscoelastic properties of fibroblast cells, both force relaxation and approach-retraction force-distance curves were analyzed using the PRL model. Interestingly, this viscoelastic model including bottom-effect corrections was analytically applied to the experimental curves measured with spherical AFM tips. The obtained results clearly evidenced the need to consider the cell thickness to avoid overestimation of the probed mechanical parameters. In addition, the viscoelastic character of cells followed a single power-law relaxation over three-decade time scales.

Overall, the results showed that force relaxation measurements, either from the individual curve or collected in mapping, constitute a powerful approach to investigate the time-dependent mechanical properties. Indeed, such experiments offered firstly a straightforward way to distinguish between two energy dissipation mechanisms, namely poroelasticity from viscoelasticity. Secondly, the procedure to implement both poroelastic and viscoelastic models for analyzing relaxation experiments was much easier than that developed to fit approach-retraction FDCs. Although analytical expressions were obtained for spherical AFM tips avoiding complex numerical calculations, analysis of FDCs requires not only correction of hydrodynamic drag forces (in the case of high tip velocities), but also accurate determination of the tip-surface contact point, the latter being more difficult to detect on soft materials than on solid ones. The proposed procedure should contribute to a more frequent use of force relaxation curves to determine the energy dissipation mechanisms and the resulting mechanical properties.

The AFM-based methodology described herein provides a solid framework to draw up a complete characterization of the time-dependent mechanical properties of living matter. Due to the structural complexity of cells and tissues, understanding their energy dissipation mechanisms (related to the experimental conditions) is an essential prerequisite toward quantitative determination of their mechanical responses, by analyzing experimental data with the appropriate theoretical models.

CRediT authorship contribution statement

Stéphane Cuenot: Writing – original draft, Validation, Methodology, Investigation, Funding acquisition, Conceptualization. **Arnaud Fillaudeau:** Writing – review & editing, Investigation, Formal analysis. **Tina Briolay:** Writing – review & editing, Investigation, Formal analysis. **Judith Fresquet:** Writing – review & editing, Investigation, Formal analysis. **Christophe Blanquart:** Writing – review & editing, Validation, Conceptualization. **Eléna Ishow:** Writing – original draft, Validation, Investigation, Funding acquisition, Conceptualization. **Agata Zykwinska:** Writing – original draft, Validation, Methodology, Investigation, Funding acquisition, Conceptualization.

Declaration of competing interest

The authors declare that they have no known competing financial interests or personal relationships that could have appeared to influence the work reported in this paper.

Acknowledgments

The French National Research Agency (ANR) is strongly acknowledged for its invaluable financial support through the AAPG generic call (grants ANR-21-CE06-0034-01/AZOTICS project and ANR-22-CE52-0005-01/SMARTIES project). "Région Pays de la Loire" is also acknowledged for its financial support through the ANR National Trajectory program (grant 27TRAJNAT ANR - n°00153485). TB was supported by a fellowship from la "Ligue contre le cancer".

Appendix A. Supplementary data

Supplementary data to this article can be found online at https://doi.org/10.1016/j.jmbbm.2024.106865.

Data availability

Data will be made available on request.

References

Berry, J.D., Biviano, M., Dagastine, R.R., 2020. Poroelastic properties of hydrogel microparticles. Soft Matter 16, 5314–5324.
Biot, M., 1956. Theory of deformation of a porous viscoelastic anisotropic solid. J. Appl. Phys. 27, 459.
Bonfanti, A., Kaplan, J.L., Charras, G., Kabla, A., 2020. Fractional viscoelastic models for power-law materials. Soft Matter 16, 6002–6020.

Chaudhuri, O., Cooper-White, J., Janmey, P.A., Mooney, D.J., Shenoy, V.B., 2020. Effects of extracellular matrix viscoelasticity on cellular behavior. Nature 584, 535–546.
Chan, E.P., Hu, Y., Johnson, P.M., Suo, Z., Stafford, C.M., 2012. Spherical indentation testing of poroelastic relaxations in thin hydrogel layers. Soft Matter 8, 1492–1498.
Cuenot, S., Alem, H., Louarn, G., Demoustier-Champagne, S., Jonas, A., 2008. Mechanical properties of nanotubes of polyelectrolyte multilayers. Eur. Phys. J. E 25, 343–348.
Cuenot, S., Bouvrée, A., Bouchara, J.-P., 2017. Nanoscale mapping of multiple lectins on cell surfaces by single-molecule force spectroscopy. Adv. Biosyst. 1, 1700050.
Cuenot, S., Gélébart, P., Sinquin, C., Colliec-Jouault, S., Zykwinska, A., 2022. Mechanical relaxations of hydrogels governed by their physical or chemical crosslinks. J. Mech. Behav. Biomed. Mater. 133, 105343.
Delavoipière, J., Tran, Y., Verneuil, E., Chateauminois, A., 2016. Poroelastic indentation of mechanically confined hydrogel layers. Soft Matter 12, 8049–8058.
Efremov, Y.M., Wang, W.-H., Hardy, S.D., Geahlen, R.L., Raman, A., 2017. Measuring nanoscale viscoelastic parameters of cells directly from AFM force-displacement curves. Sci. Rep. 7, 1541.
Efremov, Y.M., Kotova, S.L., Khlebnikova, T.M., Timashev, P.S., 2021. A time-shift correction for extraction of viscoelastic parameters from ramp-hold AFM experiments. Jpn. J. Appl. Phys. 60, SE1002.
Fillaudeau, A., Cuenot, S., Makshakova, O., Traboni, S., Sinquin, C., Hennetier, M., Bedini, E., Perez, S., Colliec-Jouault, S., Zykwinska, A., 2024. Glycosaminoglycan-mimetic infernan grafted with poly(N-isopropylacrylamide): toward a thermosensitive polysaccharide. Carbohydr. Polym. 326, 121638.
Garcia, P.D., Garcia, R., 2018a. Determination of the elastic moduli of a single cell cultured on a rigid support by force microscopy. Biophys. J. 114, 2923.
Garcia, P.D., Garcia, R., 2018b. Determination of the viscoelastic properties of a single cell cultured on a rigid support by force microscopy. Nanoscale 10, 19799.
Garcia, P.D., Guerrero, C.R., Garcia, R., 2020. Nanorheology of living cells measured by AFM-based force-distance curves. Nanoscale 12, 9133.
Hecht, F.M., Rheinlaender, J., Schierbaum, N., Goldmann, W.H., Fabry, B., Schaëffer, T. E., 2015. Imaging viscoelastic properties of live cells by AFM: power-law rheology on the nanoscale. Soft Matter 11, 4584–4591.
Hertz, H., 1881. Uber die berührung fester elastischer körper. J. Reine Angew. Math. 92, 156–171.
Hu, Y., Zhao, X., Vlassak, J.J., Suo, Z., 2010. Using indentation to characterize the poroelasticity of gels. Appl. Phys. Lett. 96, 121904.
Kollmannsberger, P., Fabry, B., 2011. Linear and nonlinear rheology of living cells. Annu. Rev. Mater. Res. 41, 75–97.
Lee, H.-P., Lippens, E., Duda, G.N., Mooney, D.J., 2016. Hydrogels with tunable stress relaxation regulate stem cell fate and activity. Nat. Mater. 15, 326–334.
Lee, H.-P., Gu, L., Mooney, D.J., Levenston, M.E., Chaudhuri, O., 2017. Mechanical confinement regulates cartilage matrix formation by chondrocytes. Nat. Mater. 16, 1243–1251.
Lee, H.-P., Alisafaei, F., Adebawale, K., Chang, J., Shenoy, V.B., Chaudhuri, O., 2021. The nuclear piston activates mechanosensitive ion channels to generate cell migration paths in confining microenvironments. Sci. Adv. 7, eabd4058.
Lee, E.H., Radok, J.R.M., 1960. The contact problem for viscoelastic bodies. J. Appl. Mech. 27, 438–444.
Lin, Y.Y., Hu, B.W., 2006. Load relaxation of a flat rigid circular indenter on a gel half space. J. Non-Cryst. Solids 352, 4034–4040.
Makshakova, O., Zykwinska, A., Cuenot, S., Colliec-Jouault, S., Perez, S., 2022. Three-dimensional structures, dynamics and calcium-mediated interactions of the exopolysaccharide, Infernan, produced by the deep-sea hydrothermal bacterium *Alteromonas infernus*. Carbohydr. Polym. 276, 118732.
Moeendarbary, E., Valon, L., Fritzsche, M., Harris, A.R., Moulding, D.A., Thrasher, A.J., Stride, E., Mahadevan, L., Charras, G.T., 2013. The cytoplasm of living cells behaves as a poroelastic material. Nat. Mater. 12, 253–261.
Moreno-Guerra, J.A., Romero-Sanchez, I.C., Martinez-Borquez, A., Tassieri, M., Stiakakis, E., Laurati, M., 2019. Model-free rheo-AFM probes the viscoelasticity of tunable DNA soft colloids. Small 15, 1904136.
Pérez-Dominguez, S., Kulkarni, S.G., Pabijan, J., et al., 2023. Reliable, standardized measurements for cell mechanical properties. Nanoscale 15, 16371.
Poon, C., 2022. Measuring the density and viscosity of culture media for optimized computational fluid dynamics analysis of in vitro devices. J. Mech. Behav. Biomed. Mater. 126, 105024.
Rigato, A., Miyagi, A., Scheuring, S., Rico, F., 2017. High-frequency microrheology reveals cytoskeleton dynamics in living cells. Nat. Phys. 13, 771–775.
Sanchez, J.G., Espinosa, F.M., Miguez, R., Garcia, R., 2021. The viscoelasticity of adherent cells follows a single power-law with distinct local variations within a single cell and across cell lines. Nanoscale 13, 16339.
Schillers, H., Rianna, C., Schäpe, J., et al., 2017. Standardized nanomechanical atomic force microscopy procedure (SNAP) for measuring soft and biological samples. Sci. Rep. 7, 5117.
Tanaka, T., Hocker, L.O., Benedek, G.B., 1973. Spectrum of light scattered from a viscoelastic gel. J. Chem. Phys. 59, 5151.
Ting, T.C., 1966. The contact stresses between a rigid indenter and a viscoelastic half-space. J. Appl. Mech. 33, 845–854.
Wei, F., Lan, F., Liu, B., Liu, L., Li, G., 2016. Poroelasticity of cell nuclei revealed through atomic force microscopy characterization. Appl. Phys. Lett. 109, 213701.
Yoon, J., Cai, S., Suo, Z., Hayward, R.C., 2010. Poroelastic swelling kinetics of thin hydrogel layers: comparison of theory and experiment. Soft Matter 6, 6004–6012.
Zhao, X., Huebsch, N., Mooney, D.J., Suo, Z., 2010. Stress-relaxation behavior in gels with ionic and covalent crosslinks. J. Appl. Phys. 107, 063509.
Zykwinska, A., Makshakova, O., Gélébart, P., Sinquin, C., Stéphant, N., Colliec-Jouault, S., Perez, S., Cuenot, S., 2022. Interactions between infernan and calcium : from the molecular level to the mechanical properties of microgels. Carbohydr. Polym. 292, 119629.